Control of polarization rotation in nonlinear propagation of fully structured light

Christopher J. Gibson, Patrick Bevington, Gian-Luca Oppo, and Alison M. Yao*
SUPA and Department of Physics, University of Strathclyde, Glasgow G4 0NG, Scotland, United Kingdom

(Received 3 November 2017; published 16 March 2018)

Knowing and controlling the spatial polarization distribution of a beam is of importance in applications such as optical tweezing, imaging, material processing, and communications. Here we show how the polarization distribution is affected by both linear and nonlinear (self-focusing) propagation. We derive an analytical expression for the polarization rotation of fully structured light (FSL) beams during linear propagation and show that the observed rotation is due entirely to the difference in Gouy phase between the two eigenmodes comprising the FSL beams, in excellent agreement with numerical simulations. We also explore the effect of cross-phase modulation due to a self-focusing (Kerr) nonlinearity and show that polarization rotation can be controlled by changing the eigenmodes of the superposition, and physical parameters such as the beam size, the amount of Kerr nonlinearity, and the input power. Finally, we show that by biasing cylindrical vector beams to have elliptical polarization, we can vary the polarization state from radial through spiral to azimuthal using nonlinear propagation.

DOI: 10.1103/PhysRevA.97.033832

I. INTRODUCTION

Vector, or fully structured light (FSL), beams [1–3] have attracted increasing attention for a number of applications. These beams consist of a vector superposition of two scalar orbital angular momentum (OAM) carrying Laguerre-Gaussian (LG) eigenmodes with orthogonal polarizations. The resultant beam has nonuniform spatial intensity, phase, and polarization distributions. The ability to control both the spatial intensity and the polarization distribution of the optical field is of use in material processing [4], in stimulated emission depletion and confocal microscopy [5–8], in optical trapping and manipulation [9,10], in atomic state preparation, manipulation, and detection [9,11,12], in optical communications [13,14], and even in classical entanglement [15–17]. Additionally, novel focusing properties associated with particular polarization distributions can lead to tighter focusing [18] and strong axial field components that are of use in microscopy [5,6], in optical trapping [9], and as a mechanism for linear accelerators [19]. It is therefore important to understand how the spatial intensity and polarization distributions can be affected, and potentially controlled, by linear and nonlinear beam propagation.

It has been shown previously that the polarization distribution of a lower-order Poincaré beam of $\ell_L = 0, \ell_R = 1$ and net OAM equal to 1 undergoes a rigid rotation of $\pi/2$ as it propagates linearly from the waist plane to the far-field zone [2]. Here we derive an analytical expression for the polarization rotation of any FSL beam during linear propagation. We show that the observed rotation is due entirely to the difference in the Gouy phase between the two eigenmodes comprising the FSL beams and explain apparent inconsistencies in the rotation of different polarization distributions. Our results are in excellent agreement with numerical simulations.

For many applications it is useful to retain a desired intensity and/or polarization distribution, for example, for modern optical technologies and high-power laser systems [20]. Beams carrying OAM are of particular interest due to their potential to carry an increased information content [13]. Although the effect of beam spreading due to diffraction during linear propagation can be mitigated, and in some cases exactly balanced, by using a self-focusing (Kerr) nonlinear medium, OAM beams are known to fragment into multiple (twice the OAM) soliton peaks during nonlinear propagation [21,22]. It has been shown that this fragmentation can be inhibited, without altering the nonlinear confinement, by using vector beams instead of scalar beams [14,23–25]. Indeed, it has been shown that cylindrical vector (CV) beams can propagate in a saturating Kerr nonlinear medium with no change to their spatial profile or their axially symmetric polarization distribution for much longer distances than the equivalent scalar beams [14]. Similar spatial confinement can be seen for FSL beams, though in this case the nonlinear propagation will affect the rotation of the polarization structure.

Here we investigate how nonlinear propagation affects the polarization distribution. We show how the magnitude and direction of the polarization rotation are affected by the spatial overlap between the two eigenmodes and how it can be controlled by modifying the effective nonlinearity via physical parameters such as the input power, the temperature of the sample, and the size of the FSL beam waist.

In addition to self-focusing, a Kerr medium also induces a cross-phase modulation between the two eigenmodes of the vector beam. We show that as the coupling tries to maximize the spatial overlap, the rotation of the polarization structure is no longer rigid. Note that, although we do not propagate our beams to the point of fragmentation, one effect of this homogenization is that the beams will fragment into equal-sized solitons.

Finally, we show that the nonlinearity not only changes the amount of polarization rotation for beams with a net OAM, but that it can also induce a rotation in beams with zero net OAM

*alison.yao@strath.ac.uk

if there is an amplitude difference between the two modes. By biasing CV beams such that they have elliptical polarization, we can vary the polarization distribution from radial through spiral to azimuthal during nonlinear propagation.

II. FULLY STRUCTURED LIGHT BEAMS

Fully structured light beams, or Poincaré beams, are constructed from a vector superposition of two scalar OAM carrying spatial transverse eigenmodes with orthogonal polarizations

$$\vec{E}(r,\phi,z) = E_L(\rho,\phi,z)\vec{e}_l + E_R(\rho,\phi,z)\vec{e}_r, \tag{1}$$

with

$$E_L = \cos(\gamma)LG_L, \quad E_R = e^{i\beta}\sin(\gamma)LG_R, \tag{2}$$

where γ and β give the relative amplitudes and phase, respectively, of the two modes. Throughout this paper we have adopted the circular polarization basis and we assume that each of the spatial modes takes the form of a Laguerre-Gaussian beam with radial index $p = 0$ [26],

$$LG_0^{\ell}(r,\phi,z) = \sqrt{\frac{2}{\pi|\ell|!}}\frac{1}{w(z)}\exp\left(\frac{-r^2}{w(z)^2}\right)\left(\frac{r\sqrt{2}}{w(z)}\right)^{|\ell|}\exp(i\ell\phi) \times \exp\left(\frac{ikr^2z}{2(z^2+z_R^2)}\right)\exp[-i(|\ell|+1)\eta(z)], \tag{3}$$

where ℓ is the OAM index of the mode, ϕ is the azimuthal angle, $z_R = k_0 w_0^2/2$ is the Rayleigh range for a beam with waist w_0 and free-space wave number k_0, $w(z) = w_0\sqrt{1+z^2/z_R^2}$ describes the linear diffraction of the beam, and $(|\ell|+1)\eta(z)$, with $\eta(z) = \tan^{-1}(z/z_R)$, is the Gouy phase [27]. If either E_L or E_R is zero, then the resultant beam is a scalar LG mode with spatially uniform right- or left-handed circular polarization, respectively. If the two modes have equal amplitude and the same OAM, the resultant beam will have spatially uniform linear polarization. If they have equal amplitude and equal but opposite OAM, however, the resultant CV beam [1,3] can have spatially varying linear polarization distributions that are radial, azimuthal, or spiral, depending on the phase difference β. The polarization of the beam will be axially symmetric about the beam's propagation axis and span the equator of the Poincaré sphere. If the two modes have different magnitudes of OAM, such that the resultant FSL beam carries a net OAM, the polarization will vary in both the angular and radial coordinates and covers all polarization states on the Poincaré sphere [2]. Note that we are working in the paraxial regime throughout, which is an excellent approximation as we are considering beam sizes that are larger than the wavelength, and that our analysis is based on vector superpositions of Laguerre-Gaussian modes, which are solutions of the paraxial wave equation in cylindrical coordinates [26]. Extension to the nonparaxial regime is nontrivial as in this case the beam polarization is a local property and changes on propagation [28]. Moreover, during propagation, a nonparaxial vortex mode will acquire a nonintegrable topological phase with no simple analytical form [29]. This tends to the Gouy phase, on which our analytical calculations are based, when the paraxial approximation is valid.

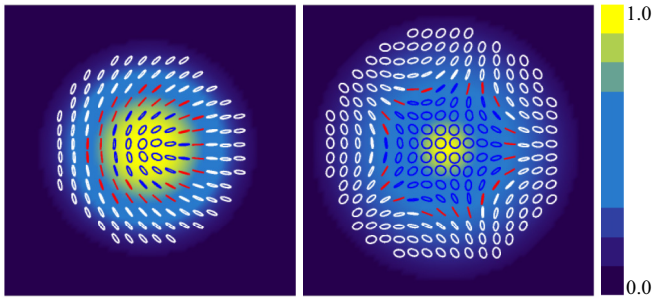

FIG. 1. Polarization distributions at the beam waist (propagation distance $z = 0$) for FSL beams with "lemon" polarization, $\ell_R = 1, \ell_L = 0$ (left), and "web" polarization, $\ell_R = -3, \ell_L = 0$ (right). White, red (light grey), blue (dark grey) lines correspond to right circular, linear, left circular polarization, respectively.

In order to map the polarization distribution on the transverse plane we use the Stokes parameters that, in the circular polarization basis, are given by [30]

$$S_0 = I = |E_R|^2 + |E_L|^2, \quad S_1 = 2\,\mathrm{Re}(E_R^* E_L),$$
$$S_2 = 2\,\mathrm{Im}(E_R^* E_L), \quad S_3 = |E_R|^2 - |E_L|^2, \tag{4}$$

where I is the intensity, the subscripts R, L denote the right and left circular components, respectively, $E_R \equiv (E_x - iE_y)/\sqrt{2}$, and $E_L \equiv (E_x + iE_y)/\sqrt{2}$). We can then calculate the ellipticity χ and orientation ψ of the polarization at each point on the transverse plane using [31]

$$\frac{S_1}{S_0} = \cos 2\chi \cos 2\psi, \quad \frac{S_2}{S_0} = \cos 2\chi \sin 2\psi, \quad \frac{S_3}{S_0} = \sin 2\chi, \tag{5}$$

which give

$$\chi = \frac{1}{2}\sin^{-1}\left(\frac{S_3}{S_0}\right) = \frac{1}{2}\sin^{-1}\left(\frac{|E_R|^2 - |E_L|^2}{|E_R|^2 + |E_L|^2}\right),$$
$$\psi = \frac{1}{2}\tan^{-1}\left(\frac{S_2}{S_1}\right) = \frac{1}{2}\tan^{-1}\left(\frac{\mathrm{Im}(E_R^* E_L)}{\mathrm{Re}(E_R^* E_L)}\right). \tag{6}$$

Typical examples of polarization distributions of FSL beams are given in Fig. 1.

Polarization rotation during linear propagation

We can calculate the orientation of the polarization at any transverse point in the field by using Eqs. (2) and (3) to re-write $\psi(z)$, Eq. (6), in terms of the constituent modes:

$$\psi(z) = \tfrac{1}{2}[(\ell_L - \ell_R)\phi - (|\ell_L| - |\ell_R|)\eta(z) - \beta]. \tag{7}$$

From this it is clear that the initial orientation of the polarization at any point $\psi(0) = \frac{1}{2}[(\ell_L - \ell_R)\phi - \beta]$ depends only on the difference in OAM of the two eigenmodes, together with any fixed initial phase difference β, and is independent of z. We note that in the case of scalar beams, where either E_L or E_R is zero, the polarization is right or left circular and so there is no direction of polarization orientation.

As the beam propagates from $z = 0$, the net polarization rotation is simply

$$\Delta\psi(z) = \psi(z) - \psi(0) = \tfrac{1}{2}\Delta|\ell_{R,L}|\eta(z), \tag{8}$$

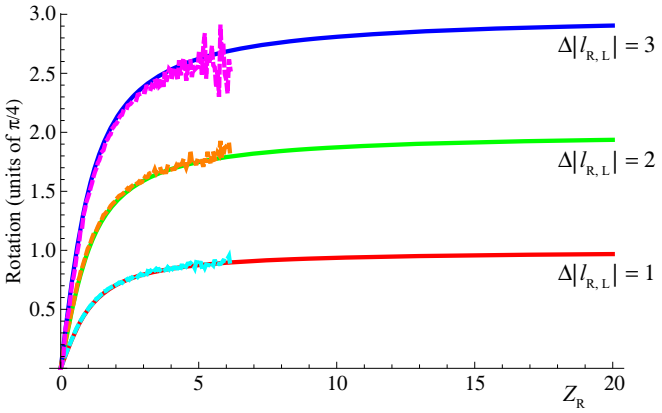

FIG. 2. Polarization rotation calculated using (8) for linear propagation from a beam waist $z = 0$ to the far field $z = 20z_R$ for FSL beams (solid lines). Dashed lines give the equivalent numerical results for $z = 0$ to $z = 6z_R$ using (12) with $\mu = 0$. Here $\Delta|\ell_{R,L}| = 1$ (red, cyan, bottom curves), 2 (green, orange, middle curves), and 3 (blue, magenta, top curves). Note that rotation is plotted in units of $\pi/4$ to clarify the asymptotic behavior.

where $\Delta|\ell_{R,L}| = |\ell_R| - |\ell_L|$. This depends only on the difference in the magnitudes of the OAM of the two modes and the Gouy phase $\eta(z)$. Note that both the polarization orientation and rotation are independent of the amplitudes of the two modes and that the amount of rotation is the same for *every* point in the transverse plane. This reduces to

$$\Delta\psi = \frac{\pi}{8}\Delta|\ell_{R,L}| \tag{9}$$

for a beam propagating from a waist plane $z = 0$ through a Rayleigh range $z = z_R$ and asymptotes to

$$\Delta\psi = \frac{\pi}{4}\Delta|\ell_{R,L}| \tag{10}$$

as the beam propagates into the far field [since $\tan^{-1}(z/z_R) \to \pi/2$ as $z \to \infty$].

Figure 2 shows the polarization rotation during linear propagation given by (8) for a number of FSL beams with different values of $\Delta|\ell_{R,L}|$ propagating from a beam waist $z = 0$ to $z = 20z_R$ (solid lines). As expected, the rotation asymptotes to $\frac{\pi}{4}\Delta|\ell_{R,L}|$. We note that this result depends only on the difference in the magnitudes of the two OAM eigenmodes, not on their particular values, and that there is no polarization rotation for cylindrical vector beams as both modes have the same magnitude of OAM and hence experience the same Gouy phase.

Figure 3 shows the polarization distributions at $z = 20z_R$ for beams with $\ell_R = 1, \ell_L = 0 \Rightarrow \Delta|\ell_{R,L}| = 1$ (left) and $\ell_R = -3, \ell_L = 0 \Rightarrow \Delta|\ell_{R,L}| = 3$ (right). Note that diffraction corresponds to a global scaling according to $w(z)$ that has been neglected for clarity.

Comparing these to the initial polarization distributions at the beam waist (Fig. 1), it appears that the polarization distribution on the left has rotated rigidly counterclockwise by $\pi/2$, as observed in [2], while the polarization distribution on the right has rotated rigidly counterclockwise by $\pi/4$. Although these results seem to contradict the predicted rotations of $\pi/4$ and $3\pi/4$, respectively, on closer inspection one can see that while

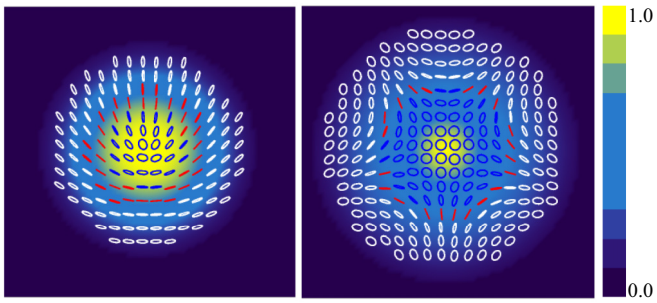

FIG. 3. Polarization distributions at $z = 20z_R$ for FSL beams with $\ell_R = 1, \ell_L = 0$ (left) and $\ell_R = -3, \ell_L = 0$ (right). White, red, and blue lines correspond to right circular, linear, and left circular polarization, respectively. Note that beam expansion due to propagation has no effect on the polarization distribution and so has been neglected for clarity.

the polarization at each point on the transverse plane is indeed as predicted by (8), the apparent rotation of the polarization structure as a whole depends on the rotational symmetry of the pattern.

We also model linear propagation of the FSL beams numerically using the paraxial equation normalized to dimensionless quantities $\rho = r/w_0$ and $\zeta = z/(2z_R)$, where w_0 is the beam waist and z_R is the Rayleigh range of the beam [21–23]

$$\frac{\partial E_{L,R}}{\partial \zeta} = \frac{i}{2}\nabla_\perp^2 E_{L,R}. \tag{11}$$

Here $E_{L,R}$ are the left- and right-circularly polarized beams and $\nabla_\perp^2$ is the Laplacian in the transverse (x,y) plane. As Fig. 2 shows, we find excellent agreement between the analytical and numerical results until the beam diffraction is too large to accurately track the polarization rotation (approximately $z = 5z_R$). Note that the effect of diffraction is more pronounced for higher-order FSL beams, resulting in increased noise as the propagation distance increases. Propagation of radial and azimuthal components of a paraxial beam along the optical axis of a uniaxial anisotropic crystal has been investigated in [32] and references therein.

III. NONLINEAR PROPAGATION

As mentioned earlier, it is possible to counteract the effect of diffraction and to control the spatial profile of the beam using a self-focussing (Kerr) nonlinearity. The usual fragmentation of scalar vortex (OAM) beams in Kerr media can be inhibited by using vector vortex or FSL beams. It has been shown that CV beams can additionally propagate with no change to their axially symmetric polarization distribution, while lower-order ($\ell = 0,1$) FSL beams experience a polarization rotation [14]. We note that azimuthally polarized, spatial, dark-soliton solutions of Maxwell's equations without OAM have been demonstrated in [33].

In order to investigate the effect of nonlinear propagation on the polarization we numerically simulated propagation of FSL beams through a Kerr medium using two coupled (2+1)-dimensional nonlinear Schrödinger equations with saturable self-focusing nonlinearity under the slowly varying envelope and paraxial approximations and normalized to dimensionless

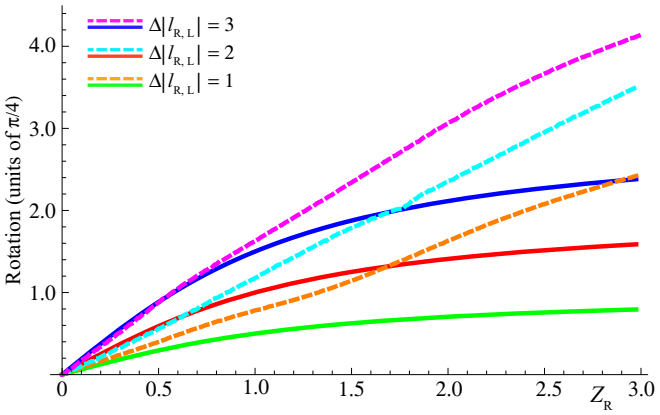

FIG. 4. Polarization rotation during nonlinear propagation from a beam waist $z = 0$ to $z = 3z_R$ using (12) with $\mu = 257.5$ and $\sigma = 19.8$ for FSL beams with $\ell_R = \pm 1, \pm 2, \pm 3$ and $\ell_L = 0$ (dashed lines). Solid lines give the corresponding analytical results for linear propagation using (8). Here $\Delta|\ell_{R,L}| = 1$ (green, orange, bottom curves), 2 (red, cyan, middle curves), and 3 (blue, magenta, top curves).

quantities $\rho = r/w_0$ and $\zeta = z/2z_R$,

$$\frac{\partial E_{L,R}}{\partial \zeta} = \frac{i}{2}\nabla_\perp^2 E_{L,R} + i\mu \frac{|E_{L,R}|^2 + 2|E_{R,L}|^2}{1 + \sigma(|E_{L,R}|^2 + 2|E_{R,L}|^2)} E_{L,R}, \tag{12}$$

where the parameters of importance are the nonlinear parameter μ and the saturation parameter σ given by

$$\mu = \frac{2k_0^2 n_2 P_0}{3n_0}, \quad \sigma = \frac{4P_0}{3I_{sat} w_0^2}, \tag{13}$$

where k_0 is the free-space wave number, n_0 and n_2 are the linear and nonlinear refractive indices ($n_2 > 0$ for self-focusing), I_{sat} is the saturation intensity, and P_0 is the power of the incident laser beam. If one neglects the beam rescaling due to diffraction, we can see from Eq. (12) that the first effect of the medium is an additional phase shift $\phi_{R,L}^{NL}$ to the orthogonal modes proportional to the nonlinear term. This results in an additional rotation $\Delta\psi_{NL}(z) \propto (\phi_L^{NL} - \phi_R^{NL})$. As the nonlinear phase shift depends on the spatial intensity of the two modes and on the cross-phase modulation, we expect the nonlinear rotation to be dependent on the magnitude of the OAM of each mode (and not just the difference in the net values). We also expect the rotation to be spatially dependent, except for the CV beams which have the same magnitude of OAM and hence the same spatial profile. We show the effect of the spatial dependence in more detail at the end of section III A, but the fact that the polarization rotation is spatially dependent then begs the question of how to measure it. An overall sense of the polarization rotation can be found either by considering a point that remains at the peak intensity of the FSL beam or by taking an average over a number of points across the beam. In cases where both eigenmodes have nonzero OAM, these two approaches are in good agreement. However, when one of the eigenmodes is a Gaussian, the transverse position of the peak changes a great deal during propagation and so the averaging method gives the best sense of the rotation behavior. For that reason we use this method for all of our nonlinear

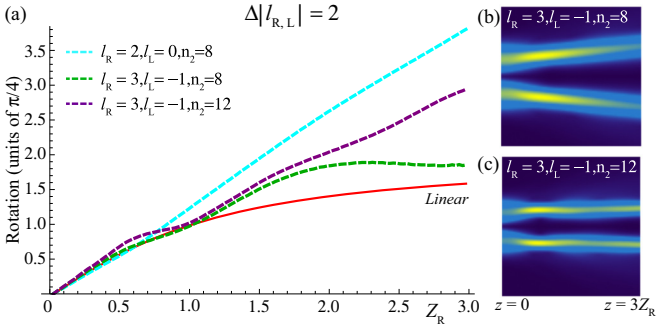

FIG. 5. (a) Polarization rotation during nonlinear propagation from a beam waist $z = 0$ for three Rayleigh ranges $z = 3z_R$ for FSL beams with a beam waist $w_0 = 100$ μm and $\Delta|\ell_{R,L}| = 2$. The cyan line (top curve) corresponds to $\ell_R = \pm 2, \ell_L = 0$ at low nonlinearity ($n_2 = 8$). Dashed lines correspond to $\ell_R = \pm 3, \ell_L = \pm 1$ at $n_2 = 8$ (green, lower middle curve) and $n_2 = 12$ (purple, upper middle curve). The red line (bottom curve) is the equivalent linear result for all superpositions. Also shown is the cross section of the spatial intensity during propagation for the FSL beams of $\ell_R = \pm 3, \ell_L = \pm 1$ at (b) $n_2 = 8$ and (c) $n_2 = 12$.

results, unless otherwise stated. Obviously, for more exact measurements, the rotation can be measured and compared at many points across the beam. In the simulations reported below, we have selected $P_0 = 7.4$ mW, $I_{sat} = 5$ W cm^{-2}, $n_2 = 8 \times 10^{-6}$ cm^2/W, and $\lambda = 780$ nm, which reproduce the experimental configuration given in [14]. We use a beam waist of 100 μm throughout (unless explicitly stated otherwise), corresponding to a Rayleigh range of approximately 4 cm. We performed numerical integrations of the propagation (12), using the split-step method with fast Fourier transforms.

A. Comparison with the linear case

To investigate the effect of the propagation in the nonlinear medium we first numerically integrated Eq. (12) for FSL beams with $\ell_R = \pm 1, \pm 2, \pm 3$ and $\ell_L = 0$, giving $\Delta|\ell_{R,L}| = 1,2,3$, respectively, with the parameters given above. Note that in order to avoid the numerical errors that occur when the beams have diffracted significantly, we present only results for propagation up to $3z_R$ throughout the remainder of the paper.

As Fig. 4 shows, in the nonlinear medium the polarization rotation no longer asymptotes but instead increases almost linearly with propagation distance. For completeness, we note that there is again no rotation for cylindrical vector beams as both modes have the same magnitude of OAM and the same spatial intensity and so they experience the same Gouy and nonlinear phase shifts.

Effect of beam composition

Unlike in the linear case, where the polarization rotation depends solely on the difference in the magnitudes of the OAM of the two eigenmodes, in the nonlinear medium the phase shift, and hence polarization rotation, depends on the spatial overlap of the eigenmodes and the cross-phase modulation between them. To demonstrate this we repeated our simulations for a number of different mode superpositions with the same difference in the Gouy phase, i.e., a fixed value of $\Delta|\ell_{R,L}| = |\ell_R| - |\ell_L|$.

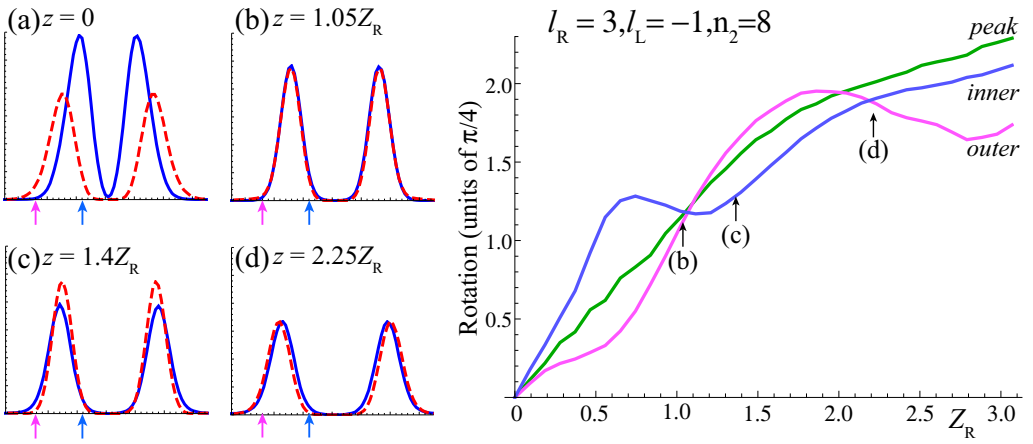

FIG. 6. (a)–(d) Cross section of modes ($\ell_R = 3$, red dashed, and $\ell_L = -1$, blue solid) with a beam waist $w_0 = 100$ μm showing the spatial overlap at various points during nonlinear propagation at low nonlinearity ($n_2 = 8$). Shown on the right is the corresponding polarization rotation. Magenta and blue lines correspond to points close to the outer edge and center of the FSL beam, respectively. The green line corresponds to the position of the peak intensity.

In Fig. 5 we show the polarization rotation for $\Delta|\ell_{R,L}| = 2$. The red line is the analytical linear result for all superpositions, as in Fig. 2, while the cyan line is the nonlinear result for a beam with $\ell_R = 2, \ell_L = 0$, as in Fig. 4. The dashed green line shows the equivalent result but for a beam with $\ell_R = 3, \ell_L = -1$ (green). Note that similar behavior is seen for the beam with $\ell_R = 4, \ell_L = -2$, but this is omitted for clarity. We see a significant change in the behavior of the polarization rotation between the lowest-order FSL beam $\ell_L = 0$ and the higher-order beams $|\ell_L| > 0$. In particular, we note that the higher-order beam experiences less polarization rotation overall: There are regions during the propagation where the polarization rotation seems to stop, or even change direction, and the rotation appears to asymptote with increasing propagation distance.

There are two important phenomena affecting the behavior of the polarization rotation: the intensity of the modes and their spatial overlap. In Fig. 5 we plot the cross section of the beam intensity of the $\ell_R = 3, \ell_L = -1$ mode at two different values of the nonlinearity, $n_2 = 8$ (top) and $n_2 = 12$ (bottom). It is clear that there is still significant diffraction for $n_2 = 8$, and the corresponding reduction in intensity results in less of a nonlinear phase shift and leads to the asymptotic behavior of the rotation [green line in Fig. 5(a)]. At $n_2 = 12$, however, the beam is quite well confined and there is also a more consistent mode overlap. In this case we almost recover the rotation experienced by the lowest-order mode [dashed purple line in Fig. 5(a)].

As mentioned earlier, the nonlinear polarization rotation also depends on the cross-phase modulation and hence on the spatial overlap of the eigenmodes. An overall sense of the behavior of the polarization rotation can usually be found by tracking the polarization at a point that remains at the peak intensity of the FSL beam. However, when one of the eigenmodes is a Gaussian, the transverse position of the peak changes significantly during propagation and so a better method is to average the results over a number of points across the beam. For applications requiring more exact knowledge of the polarization state at each point on the transverse plane, the polarization rotation can be compared at various points across the beam. To demonstrate the effect of the cross-phase modulation term we consider a beam with eigenmodes of $\ell_R = 3$ and $\ell_L = -1$. As the cross-phase modulation term is asymmetric unless $|\ell_R| = |\ell_L|$ and contains a saturating term, the mode sizes will oscillate during propagation with corresponding variations in the spatial overlap. The polarization rotation at each point will therefore depend on its location on the transverse plane. This is demonstrated in Fig. 6 for propagation of a FSL beam with $\ell_R = 3, \ell_L = -1$ at low nonlinearity ($n_2 = 8$). At the start of the propagation [see Fig. 6(a)], points on the outer edge of the beam (magenta) see more right-circularly polarized light while points closer to the center (blue) see more left-circularly polarized light and thus their polarizations rotate in opposite directions. When the modes overlap exactly [Fig. 6(b)] the modes experience the same nonlinear phase shift and so there is no net nonlinear rotation. If the beams remain locked like this there is a corresponding plateau in the rotation curve (see, for example, Fig. 5, green line). As the modes oscillate net left- or right-circularly polarized light can swap, resulting in polarization rotation changing direction [Fig. 6(c)]. Note that as the beam continues to propagate the effect of the nonlinearity is to try to maintain the spatial overlap of the two modes. The locked beams then propagate with a constant small rotation depending on the overlap until they fragment into solitons [21,22] [Fig. 6(d)].

B. Control of polarization rotation

In addition to understanding how the state of polarization is affected by propagation, it may be useful to be able to control it. Linearly the polarization rotation can be controlled by choosing the eigenmodes of the FSL beam to give a specific difference in the magnitudes of the OAM ($\Delta|\ell_{R,L}|$), as shown in Fig. 2, and by choosing the beam size to control the Rayleigh range.

Nonlinearly, the amount and direction of the nonlinear polarization rotation also depends on the spatial overlap and intensity of the eigenmodes. These can be controlled both by the choice of eigenmodes (see Fig. 5) and by changing experimental parameters such as the power of the FSL beam, the temperature of the medium [14], and the size of the FSL

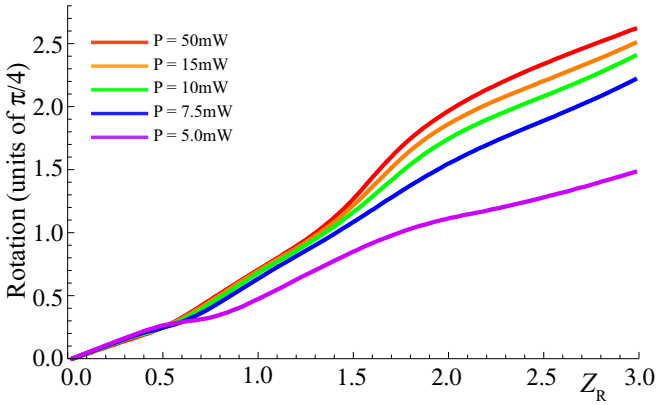

FIG. 7. Polarization rotation of $\ell_R = 1$ and $\ell_L = 0$ beam during nonlinear propagation from a beam waist $z = 0$ to $z = 3z_R$ for FSL beams with input powers of 5 mW (purple), 7.5 mW (blue), 10.0 mW (green), 15.0 mW (orange), and 50.0 mW (red), where the referenced curves are in order from bottom to top.

beam to control the nonlinear parameter μ and the saturation parameter σ [Eq. (13)] and hence the confinement of the beam.

For example, Fig. 7 shows how the polarization rotation of the $\ell_R = 1$ and $\ell_L = 0$ beam changes as we increase the input power P. This increases both the nonlinear response and the saturation parameter leading to an enhanced polarization rotation at the output.

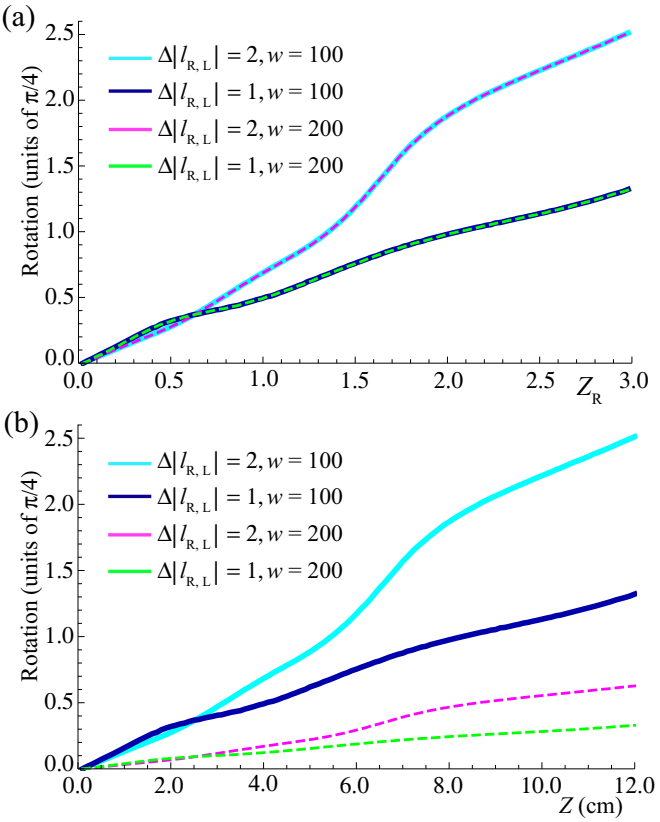

FIG. 8. Polarization rotation during nonlinear propagation for FSL beams with $\Delta|\ell_{R,L}| = 1,2$ and waists of 100 μm (dark - blue lower solid, cyan - upper solid) and 200 μm (green - lower dashed, magenta - upper dashed): (a) rotation versus number of Rayleigh lengths and (b) rotation versus distance (cm). In both cases $\mu = 257.5$ and $\sigma = 19.8$.

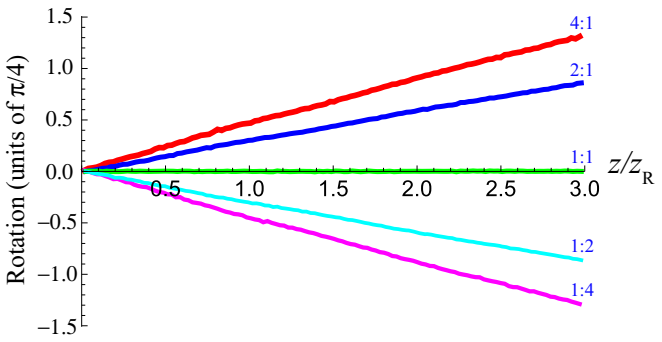

FIG. 9. Nonlinear polarization rotation for propagation of a cylindrical vector beam with $|\ell_{R,L}| = 1$ over $3z_R$. The parameter γ in (2) is chosen such that $|E_R|:|E_L|$ is 4:1 (red, top curve), 2:1 (blue, upper middle curve), 1:1 (green, middle curve), 1:2 (cyan, lower middle curve), and 1:4 (magenta, bottom curve).

As before, the size of the FSL beam can also be used to control the Rayleigh range. In Fig. 8 we plot the polarization rotation during nonlinear propagation from a beam waist $z = 0$ to $z = 3z_R$ for FSL beams with waists of 100 μm and $\Delta|\ell_{R,L}| = 1,2$ (dark blue, cyan) using (12) with $P = 7.44$ mW and $n_2 = 8 \times 10^{-6}$ W cm^{-2} such that $\mu = 257.5$ and $\sigma = 19.8$. Equivalent results exist for beams with waists of 200 μm (green, magenta) and with rescaled experimental parameters $P = 29.8$ mW and $n_2 = 2 \times 10^{-6}$ W cm^{-2} such that σ and μ are unchanged. We consider two superpositions of FSL beams ($\ell_R = 1, \ell_L = 0$ and $\ell_R = 2, \ell_L = 1$) and show that the results for the two different beam waists match in both cases if we plot rotation versus the number of Rayleigh lengths propagated [Fig. 8(b)]. If, however, we plot the same results as a function of distance [Fig. 8(b)], we can see that by doubling the beam waist, and hence increasing z_R by a factor 4, the rotation of the larger beam is correspondingly decreased by a factor 1/4.

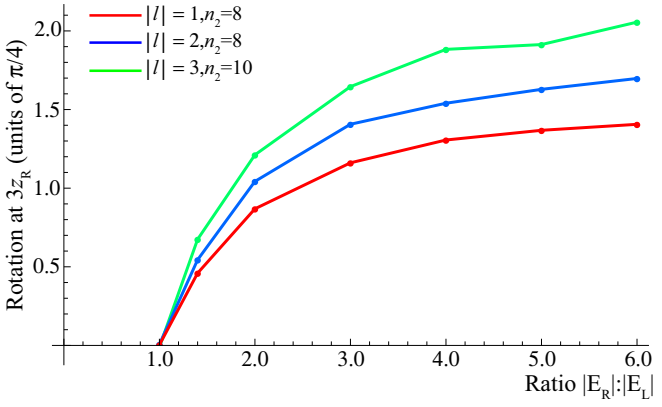

FIG. 10. Nonlinear polarization rotation at $3z_R$ as a function of bias for biased CV beams with $|\ell_{R,L}| = 1,2,3$ (red - bottom, blue - middle, and green - top, respectively).

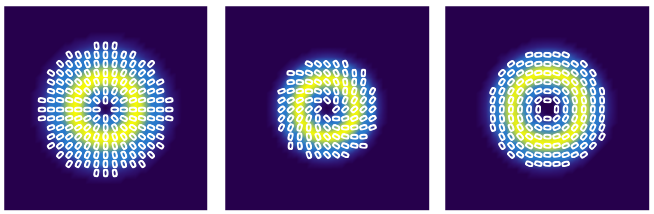

FIG. 11. Radially elliptically polarized vector beam with $|\ell_{R,L}| = 1$ and $|E_R|:|E_L| = 4{:}1$, from left to right, at a beam waist $z = 0$ and after nonlinear propagation over $z = 1.3Z_R$ and over $z = 2.5Z_R$. There is little change to the spatial profile of the beam during propagation, but the polarization changes from radial through spiral to azimuthal.

C. Biased vector beams $\gamma \neq \pi/4$

While many applications of cylindrical vector beams use spatially varying linear polarization (radial or azimuthal), beams with azimuthally varying elliptical polarization allow the space-variant spin in the beam to be transferred to the atomic medium, thus offering a unique way to manipulate atoms spatially [12]. Such elliptically polarized FSL beams can be produced by changing the relative amplitudes of the two eigenmodes of a cylindrical vector beam [i.e., by changing the value of γ in Eq. (2)]. As we have already mentioned, equal-amplitude CV beams do not experience any polarization rotation during propagation, linearly or nonlinearly, as both components have the same magnitude of OAM and hence experience the same Gouy phase and the same spatial intensity distribution. However, when elliptically polarized, or biased, CV beams are propagated in the nonlinear medium we find that the polarization distributions do rotate and that the amount and direction of the rotation are dependent on the ellipticity of the polarization. This is clearly shown in Fig. 9, where $|\ell_R| = |\ell_L| = 1$ and γ in Eq. (2) has been chosen such that $|E_R|:|E_L|$ is 4:1 (red), 2:1 (blue), 1:1 (green), 1:2 (cyan), and 1:4 (magenta).

Note that as the bias is increased the beams become more "scalar" as the contribution of the second beam becomes negligible, and the polarization becomes circular. In this case we recover the behavior demonstrated in [14], where the scalar beam is shown to fragment more quickly than the corresponding vector beam. As Fig. 10 shows, the amount of rotation saturates as the bias increases. The rotation may also be increased by using higher-order CV beams, but as these diffract more for the same experimental parameters, a higher nonlinearity is required in order to keep the beams confined.

One effect of this rotation is the conversion of radial (or azimuthal) elliptical polarization to azimuthal (or radial) with minimal changes to the spatial profile of the beam, as shown in Fig. 11. By choosing the bias and the propagation distance for a given beam waist, we can control the polarization of the beam with no polarization optics.

IV. CONCLUSION

Knowing how the spatial polarization distribution of a beam is affected by propagation is of importance in many applications that depend on the state of polarization. We have analytically calculated the polarization rotation of fully structured light beams during linear propagation and shown that the observed rotation is due entirely to the difference in Gouy phase between the two eigenmodes comprising the FSL beams. This allows the exact polarization state at a particular propagation distance to be controlled simply by choosing the eigenmodes of the FSL beam and the beam size. Moreover, we have shown that polarization rotation is also affected by propagation through a self-focusing (Kerr) nonlinear medium and that this can be controlled by changing the eigenmodes of the superposition and physical parameters such as the beam size, the amount of Kerr nonlinearity, and the input power. In addition, the ability to control both the intensity and polarization of FSL beams may provide a useful method for applications in micromachining and microscopy [4,34]. Finally, we have shown that by biasing cylindrical vector beams to have elliptical polarization, we can vary the polarization state from radial through spiral to azimuthal using nonlinear propagation.

ACKNOWLEDGMENTS

We would like to acknowledge support from the Engineering and Physical Sciences Research Council DTA Grant No. EP/M506643/1 and from the Carnegie Trust for the Universities of Scotland. A.M.Y. would like to thank the Leverhulme Trust for the award of a Leverhulme Trust Research Project Grant No. RPG-2017-048 to further support this research.

[1] Q. Zhan, Adv. Opt. Photon. **1**, 1 (2009).
[2] A. M. Beckley, T. G. Brown, and M. A. Alonso, Opt. Express **18**, 10777 (2010).
[3] E. J. Galvez, S. Khadka, W. H. Schubert, and S. Nomoto, Appl. Opt. **51**, 2925 (2012).
[4] A. V. Nesterov and V. G. Niziev, J. Phys. D **33**, 1817 (2000).
[5] K. I. Willig, S. O. Rizzoli, V. Westphal, R. Jahn, and S. W. Hell, Nature (London) **440**, 935 (2006).
[6] P. Török and P. R. T. Munro, Opt. Express **12**, 3605 (2004).
[7] K. S. Youngworth and T. G. Brown, Opt. Express **7**, 77 (2000).
[8] S. N. Khonina and I. Golub, J. Opt. Soc. Am. A **29**, 2242 (2012).
[9] L. Novotny, M. R. Beversluis, K. S. Youngworth, and T. G. Brown, Phys. Rev. Lett. **86**, 5251 (2001).
[10] A. LaPorta and M. D. Wang, Phys. Rev. Lett. **92**, 190801 (2004).
[11] B. Sick, B. Hecht, and L. Novotny, Phys. Rev. Lett. **85**, 4482 (2000).
[12] F. K. Fatemi, Opt. Express **19**, 25143 (2011).
[13] N. Bozinovic, Y. Yue, Y. Ren, M. Tur, P. Kristensen, H. Huang, A. E. Willner, and S. Ramachandran, Science **340**, 1545 (2013).
[14] F. Bouchard, H. Larocque, A. M. Yao, C. Travis, I. De Leon, A. Rubano, E. Karimi, G.-L. Oppo, and R. W. Boyd, Phys. Rev. Lett. **117**, 233903 (2016).
[15] C. Gabriel, A. Aiello, W. Zhong, T. G. Euser, N. Y. Joly, P. Banzer, M. Förtsch, D. Elser, U. L. Andersen, C. Marquardt, P. S. J. Russell, and G. Leuchs, Phys. Rev. Lett. **106**, 060502 (2011).

[16] X.-F. Qian and J. H. Eberly, Opt. Lett. **36**, 4110 (2011).
[17] S. Berg-Johansen, F. Töppel, B. Stiller, P. Banzer, M. Ornigotti, E. Giacobino, G. Leuchs, A. Aiello, and C. Marquardt, Optica **2**, 864 (2015).
[18] R. Dorn, S. Quabis, and G. Leuchs, Phys. Rev. Lett. **91**, 233901 (2003).
[19] P. Serafim, P. Sprangle, and B. Hafizi, IEEE Trans. Plasma Sci. **28**, 1155 (2000).
[20] R. Y. Chiao, E. Garmire, and C. H. Townes, Phys. Rev. Lett. **13**, 479 (1964).
[21] W. J. Firth and D. V. Skryabin, Phys. Rev. Lett. **79**, 2450 (1997).
[22] A. S. Desyatnikov and Y. S. Kivshar, Phys. Rev. Lett. **87**, 033901 (2001).
[23] M. S. Bigelow, Q.-H. Park, and R. W. Boyd, Phys. Rev. E **66**, 046631 (2002).
[24] M. S. Bigelow, P. Zerom, and R. W. Boyd, Phys. Rev. Lett. **92**, 083902 (2004).
[25] A. S. Desyatnikov, D. Mihalache, D. Mazilu, B. A. Malomed, and F. Lederer, Phys. Lett. A **364**, 231 (2007).
[26] S. M. Barnett and R. Zambrini, in *Quantum Imaging*, edited by K. I. Kolobov (Springer, Singapore, 2007), p. 284.
[27] R. W. Boyd, J. Opt. Soc. Am. **70**, 877 (1980).
[28] D. N. Pattanayak and G. P. Agrawal, Phys. Rev. A **22**, 1159 (1980).
[29] A. V. Volyar, V. G. Shvedov, and T. A. Fadeeva, Opt. Spectrosc. **90**, 93 (2001).
[30] M. R. Dennis, K. O'Holleran, and M. J. Padgett, Prog. Opt. **53**, 293 (2009).
[31] B. E. A. Saleh and M. C. Teich, *Fundamentals of Photonics* (Wiley, New York, 2007).
[32] G. Cincotti, A. Ciattoni, and C. Sapia, Opt. Commun. **220**, 33 (2003).
[33] A. Ciattoni, B. Crosignani, P. Di Porto, and A. Yariv, Phys. Rev. Lett. **94**, 073902 (2005).
[34] K. J. Mitchell, S. Turtaev, M. J. Padgett, T. Čižmàr, and D. B. Phillips, Opt. Express **24**, 29269 (2016).